

Nanoscale

Accepted Manuscript



This is an *Accepted Manuscript*, which has been through the Royal Society of Chemistry peer review process and has been accepted for publication.

Accepted Manuscripts are published online shortly after acceptance, before technical editing, formatting and proof reading. Using this free service, authors can make their results available to the community, in citable form, before we publish the edited article. We will replace this *Accepted Manuscript* with the edited and formatted *Advance Article* as soon as it is available.

You can find more information about *Accepted Manuscripts* in the [Information for Authors](#).

Please note that technical editing may introduce minor changes to the text and/or graphics, which may alter content. The journal's standard [Terms & Conditions](#) and the [Ethical guidelines](#) still apply. In no event shall the Royal Society of Chemistry be held responsible for any errors or omissions in this *Accepted Manuscript* or any consequences arising from the use of any information it contains.



Nanoscale

PAPER

Organic crystal-binding peptides: Morphology control and one-pot formation of protein-displaying organic crystals

Teppei Niide,^a Kyohei Ozawa,^a Hikaru Nakazawa,^a Daniel Oliveira,^{a, b} Hitoshi Kasai,^c Mari Onodera,^a Ryutaro Asano,^a Izumi Kumagai^a and Mitsuo Umetsu^{*, a, b}

Received 00th January 20xx,
Accepted 00th January 20xx

DOI: 10.1039/x0xx00000x

www.rsc.org/

Crystalline assemblies of fluorescent molecules have different functional properties than the constituent monomers, as well as unique optical characteristics that depend on the structure, size, and morphological homogeneity of the crystal particles. In this study, we selected peptides with affinity for the surface of perylene crystal particles by exposing a peptide-displaying phage library in aqueous solution to perylene crystals, eluting the surface-bound phages by means of acidic desorption or liquid-liquid extraction, and amplifying the obtained phages in *Escherichia coli*. One of the perylene-binding peptides, PeryBP_{b1}: VQHNTKYSVVIR, selected by this biopanning procedure induced perylene molecules to form homogenous planar crystal nanoparticles by means of a poor solvent method, and fusion of the peptide to a fluorescent protein enabled one-pot formation of protein-immobilized crystalline nanoparticles. The nanoparticles were well-dispersed in aqueous solution, and Förster resonance energy transfer from the perylene crystals to the fluorescent protein was observed. Our results show that the crystal-binding peptide could be used for simultaneous control of perylene crystal morphology and dispersion and protein immobilization on the crystals.

Introduction

In biological milieu, peptides and proteins selectively recognize interfacial surfaces of biomolecules *via* multiple interactions, such as hydrogen bonds, salt bridges, and hydrophobic packing. Recently, combinatorial library approaches have been used to generate peptides with affinity for nonbiological materials such as metals,^{1–3} metal oxides,^{4–6} and polymeric plastics.⁷ These material-binding peptides are expected to be useful for bottom-up processes in the field of bionanotechnology, such as patterning and assembly of nanomaterials and biomolecules,^{8–12} biofunctionalization of nanoparticles,^{13,14} and synthesis of nanomaterials.^{5,15–17}

Of particular interest are peptides that can bind organic semiconductor materials. These materials, which have unique optical, electrical, and chemical properties, are typically polymers or assemblies of π -conjugated small molecules. Compared to polymers, crystals of π -conjugated molecules have higher chromophore packing density, more-stable molecular orientation, and superior photochemical reactivity.¹⁸

The physical properties of molecular assemblies depend not only on the structure of the constituent molecules but also on the size, shape, and crystallinity of the assembly itself.^{19–23} Organic semiconductor materials based on perylene, which has a high fluorescence quantum yield and good chemical stability, are among the highest performing organic semiconductor materials,^{24–26} and perylene-based semiconductors are used in complementary logic circuits²⁷ and organic solar cells.²⁸ Furthermore, the optoelectronic properties of perylene nanocrystals have been shown to depend on crystal size and morphology.^{20,29}

In this study, we used a peptide-displaying phage library to select peptides with affinity for perylene crystal particles, and an acidic desorption method or a liquid-liquid extraction method was used to separate the perylene from the phages. One of the selected peptides changed the size and structure of perylene crystal particles formed by means of a poor solvent method, and the peptide-bound crystal particles could be easily dispersed in water. Dispersion of organic nanocrystals in solution makes them easier to handle for constructing devices.³⁰ The perylene-binding peptide was used to immobilize a fluorescent protein on perylene crystals. The resulting suspensions of nanoparticles were transparent (indicating high dispersion of the nanoparticles), and Förster resonance energy transfer (FRET) from perylene to the protein occurred. Thus, we showed that peptides can recognize the surface of crystalline molecular assemblies and can be used to control the morphology, dispersion, and surface function of the assemblies simultaneously.

^a Department of Biomolecular Engineering, Graduate School of Engineering, Tohoku University, 6-6-11 Aoba, Aramaki, Aoba-ku, Sendai 980-8579, Japan.

^b WPI-Advanced Institute for Materials Research, Tohoku University, 2-1-1 Katahira, Aoba-ku, Sendai, 980-8577, Japan.

^c Institute of Multidisciplinary Research for Advanced Materials, Tohoku University, 2-1-1 Katahira, Aoba-ku, Sendai, 980-8577, Japan.

† Electronic Supplementary Information (ESI) available: Schematic representation of PeryBP_{b1}-fused DsRed-Monomer, fluorescence spectra of perylene crystals and DsRed-Monomer, and emission spectra of DsRed-Monomer at various excitation wavelengths. See DOI: 10.1039/x0xx00000x

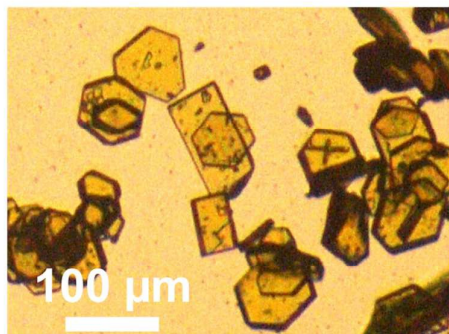


Fig. 1 Microscopy image of perylene crystals formed by recrystallization. Perylene powder were dissolved 70°C benzene, and then the temperature was slowly decrease until 25°C for crystal formation. Resulting perylene crystals were used for phage display, adsorption experiment and FRET analysis.

Experimental

Preparation of perylene crystals by recrystallization

Perylene powder (>95.0%, Wako Pure Chemical Industries, Osaka, Japan) in benzene at a concentration of 20 mM was heated at 70°C with stirring. After the perylene dissolved, the solution was gradually cooled to 25°C with stirring, and the precipitated perylene crystals were collected by filtration. A microscopy image (CX31, Olympus, Tokyo, Japan) of the perylene crystals is shown in Fig. 1.

Selection of peptides with affinity for perylene crystal particles

A phage library consisting of random 12-mer peptides ($\sim 2 \times 10^9$) displayed on the minor coat protein (pIII) of the M13 bacteriophage (Ph.D.-12 Phage Display Peptide Library Kit, New England BioLabs, Beverly, MA, USA) was used to obtain peptides with affinity for perylene crystal particles. Phages ($\sim 10^{11}$) were mixed with 5 mg of perylene crystal particles in 1 mL of a 50 mM sodium phosphate solution (pH 7.5) containing 150 mM NaCl and 0.5% v/v Tween-20, and the solution was incubated at room temperature with gentle agitation for 10 min. The perylene crystal particles were washed 10 times with the sodium phosphate solution to remove unbound phages.

The washed perylene crystal particles with bound phages were then immersed in 1 mL of 200 mM glycine-HCl (pH 2.2) containing 1 mg mL⁻¹ bovine serum albumin for 10 min at room temperature with gentle agitation to elute the bound phages. After centrifugation, the phages in the supernatant were amplified by infection of *Escherichia coli*. The phages that remained bound to the perylene crystal particles after treatment with the acidic solution were also amplified by direct addition of the particles to a culture medium containing *E. coli*. After several rounds of this biopanning procedure (selection, elution, and amplification), the peptide sequences displayed on the isolated phases were analyzed.

1. Perylene-binding peptide–GGGSAGSAGSAAGSGEF–DsRed-Monomer
2. MGGGSAGSAGSAAGSGEF–DsRed-Monomer

Fig. 2 Schematic representations of the perylene-binding peptide-fused DsRed-Monomer (1) and -unfused DsRed-Monomer (2).

We also used a liquid–liquid extraction method to elute the phages from the perylene crystal particles. Specifically, a mixture of benzene and 50 mM sodium phosphate solution (pH 7.5) containing 150 mM NaCl and 0.5% v/v Tween-20 was added to the washed peptide-bearing perylene crystals. After gentle agitation at room temperature for 10 min, the mixture was centrifuged to induce phase separation, and then the phages in the aqueous phase were amplified by infection of *E. coli*.

Assay of the binding affinity of the selected peptides

The sequences of the peptides selected by the above-described method were determined, and the identified peptides were then purchased with a fluorescein label at the N-terminus via a glycine linker (GGGS) and the C-terminus amidated (Sigma-Aldrich, St. Louis, MO, USA). A solution of each fluorescein-labeled peptide in 1 mL of 10 mM sodium phosphate at pH 7.5 was mixed with 5 mg of perylene crystal particles at room temperature for 10 min in the dark. After centrifugation, the fluorescence in the supernatants was measured with a fluorescence spectrophotometer (F-2500, Hitachi Science & Technology, Tokyo, Japan) at an excitation wavelength of 495 nm to estimate the concentrations of peptides bound to the perylene crystals. Dissociation constants and saturation adsorption amounts were calculated by Langmuir adsorption isotherm.

Preparation of peptide–peryene crystals via reprecipitation

Peptide–peryene crystals were prepared by means of a reprecipitation method as follows.^{31,32} Ultrapure water (>18 MΩ, 4 mL) containing peptide at a concentration of 0–100 μM was vigorously stirred, and 1 mL of a dimethylsulfoxide solution of perylene (10 mM) was added to the stirred solution. After 1 h with stirred, the colloidal crystals that formed were collected on an alumina membrane (pore size, 0.02 μm; Anodisc, GE Healthcare Bio-Science, Piscataway, NJ, USA), washed 3 times with ultrapure water, and then dried under vacuum. The morphologies of the resulting colloidal crystal particles were determined by means of field emission scanning electron microscopy (SEM; S-4800, Hitachi Science & Technology) and field emission scanning transmission electron microscopy (TEM; HD-2700, Hitachi Science & Technology). Prior to SEM analysis, the crystals were dried on a carbon sample stage, and then the crystals were coated with a thin layer of osmium.

Construction of an expression vector for peptide-fused DsRed-Monomer

The gene fragment coding the monomeric red fluorescent protein from *Discosoma* (DsRed-Monomer) with a GGGGAGSAGSAAGSGEF linker^{33,34} was amplified with the pDsRed-Monomer expression vector (Takara Bio Inc., Shiga, Japan) using the following primers: DsRMF, 5'-NNNGGATCCGCTGGCTCCGCTGCTGGTCTGGCGAATTTATGGACAACACCGAGGACG-3'; DsRMB, 5'-NNNGAATTCCTACTGGGAGCCGGAGTGG-3'. The amplified fragments were digested with *Bam*HI and *Eco*RI and inserted into a similarly digested pET20b(+) vector. The vector containing the DsRed-Monomer fragments was digested with *Nde*I and *Bam*HI, and the oligonucleotide coding the peptide with affinity for perylene crystal particles was inserted to express peptide-fused DsRed-Monomer (Fig. 2).

Preparation of recombinant DsRed-Monomer

E. coli (BL21 [DE3] strains, Life Technologies, Carlsbad, CA, USA) was transformed with the expression vector encoding recombinant DsRed-Monomer (DsRed-Monomer or peptide-fused DsRed-Monomer). Transformed *E. coli* cells were inoculated in 3 mL of LB medium containing 100 mg L⁻¹ of ampicillin sodium overnight at 37°C, and then the culture medium was poured into 250 mL of 2 × YT medium containing 100 mg L⁻¹ of ampicillin sodium. Isopropyl-β-D-thiogalactopyranoside was added to a final concentration of 1.0 mM when the optical density of the culture medium at 600 nm (OD₆₀₀) reached 0.8, and the culture medium was further incubated for 16 h at 25°C. The harvested cells were centrifuged at 5,800g for 20 min at 4°C, and the pellet was resuspended in low-salt buffer (10 mM sodium phosphate buffer, pH 7.5). After ultrasonication, the suspension was centrifuged, and the supernatant was fractionated by means of anion exchange chromatography (HiTrap Q HP column, GE Healthcare Bio-Science) using a linear NaCl gradient (10 mM sodium phosphate buffer, pH 7.5) from 0 to 500 mM. The fractions containing recombinant DsRed-Monomer were further purified by means of size-exclusion chromatography (Hiload Superdex 200-pg column 26/60; GE Healthcare Bio-Science) using 50 mM sodium phosphate buffer (pH 7.5) containing 200 mM NaCl. Before use, the recombinant DsRed-Monomer was dialyzed against 10 mM sodium phosphate buffer (pH 7.5).

Assay of the binding affinity of the recombinant DsRed-Monomer

A solution of various concentration of PeryBP_{b1}-fused DsRed-Monomer (0–1.0 μM) in 1 mL of 10 mM sodium phosphate at pH 7.5 was mixed with 5 mg of perylene crystal particles at room temperature for 10 min in the dark. After centrifugation at 8,000g for 5 min, the fluorescence in the supernatants was measured with a fluorescence spectrophotometer (F-2500, Hitachi Science & Technology) at an excitation wavelength of 556 nm to estimate the concentrations of the recombinant DsRed-Monomer bound to the perylene crystals. Equilibrium

dissociation constants and saturation adsorption amounts were calculated by Langmuir adsorption isotherm.

Preparation of DsRed-Monomer-immobilized perylene crystals

DsRed-Monomer-immobilized perylene crystals were prepared in two methods: step-by-step and one pot preparations. For step-by-step method, 10 mg of perylene crystals formed by recrystallization were mixed with 10 mM sodium phosphate (pH 7.5) containing 0–50 μM DsRed-Monomer with perylene-binding peptide fused at the N-terminus. The reaction mixtures were agitated for 10 min at room temperature in the dark. After centrifugation at 8,000g for 5 min, the precipitates were dried on quartz glass under vacuum to carry out FRET analysis.

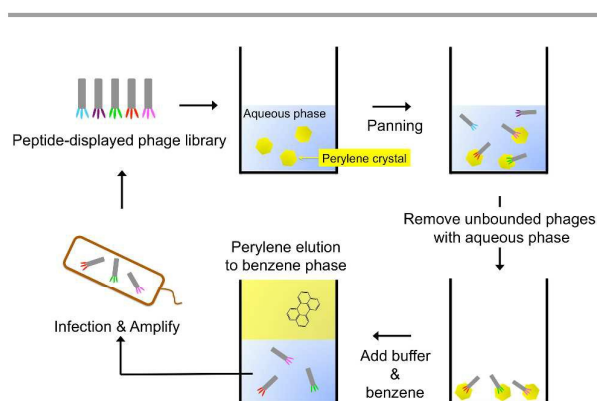
For one pot method, 4 mL of 10 mM sodium phosphate buffer (pH 7.5) containing the peptide-fused DsRed-Monomer at the concentrations of 0–2.0 μM was vigorously stirred, and 1 mL of a dimethylsulfoxide solution containing perylene (10 mM) was added to the stirred solution. After 1 h incubation with stirred in the dark, the size distribution of the formed colloidal crystals were measured with dynamic light scattering (DLS) instrument (Zetasizer Nano-ZS, Malvern, Worcestershire, UK). The crystals were collected on an alumina membrane (pore size, 0.02 μm; Anodisc, GE Healthcare Bio-Science), and after washing three times they were dried under vacuum on a carbon sample stage for measuring SEM analysis and on quartz glass for FRET analysis.

FRET analysis

The fluorescence of the DsRed-Monomer-immobilized perylene crystals dried on quartz glass were measured with an F-2500 fluorescence spectrophotometer (Hitachi Science & Technology) at an excitation wavelength of 400 nm, and the fluorescence from 500 nm to 700 nm.

Results

Phage-based selection of peptides with affinity for the surface of perylene crystal particles



Scheme 1 Schematic illustration of biopanning with liquid-liquid extraction.

Table 1 Characteristics of perylene crystal-binding peptides obtained after the second and third rounds of biopanning.

Round	Sample code	Sequence	pI ^[a]	Hydropathy index ^[b]	No. of identified clones/total no. of picked clones	K _d ^[c] (μM)	W _s ^[c] (pmol/mg)
2	PeryBP _{g1}	HWTWSPACTFHA	6.91	-0.258	24/32	-	19 ^[e]
2	PeryBP _{g2}	RHPPTLDPYYTM	6.74	-1.192	7/32	-	11 ^[e]
2	PeryBP _{g3}	TGLETHYRLMKS ^[d]	7.90	-0.550	1/32	-	-
3	PeryBP _{b1}	VQHNTKYSVVIR	9.99	-0.358	22/22	1.2	303

[a] pIs were calculated using the ExpASY Compute pI/Mw tool available at http://web.expasy.org/compute_pi/.

[b] Hydropathy indexes were calculated using the GRAVY (grand average of hydropathy) calculator available at <http://www.gravy-calculator.de/>.

[c] Equilibrium dissociation constants (K_d) and saturated bound amount (W_s) values were estimated from Langmuir plot by using the data in Fig. 3.

[d] The binding properties of this peptide were not analyzed.

[e] Estimated from the saturation point in Fig. 3.

To select peptides with affinity for the surface of perylene crystal particles, we used a biopanning method with a phage library system based on random 12-mer peptides fused to the minor coat protein (pIII) of the M13 bacteriophage. After obtaining perylene crystals by means of recrystallization (Fig. 1), we mixed the phage library with the crystal particles and then removed the unbound phages by washing with an aqueous solution. The residual phages bound to the crystal particles were eluted either by desorption with an acidic (pH 2.2) solution or by liquid-liquid extraction. The former method is the most commonly used elution method.^{2,3} In the latter method, the phage-bound perylene crystal particles were dissolved in a mixture of benzene and water; the perylene dissolved in the benzene phase, and the phages partitioned to the water phase (Scheme 1).

The acidic solution obtained by the desorption method and the perylene crystals left behind after removal of the acidic solution were incubated with *E. coli*, respectively, to generate phage plaques. After the second round of selection, only the *E. coli* infected by addition of the crystal particles made plaques; and after 3 rounds of selection, neither the bacteria infected with the acidic solution nor the bacteria infected with the crystals made plaques. It is possible that the acidic solution did not completely desorb the bound phages from the perylene crystal particles and that the particle-bound phages had low infectivity to *E. coli*. In contrast, the mixture of benzene and water completely dissolved the perylene crystal particles, and the perylene molecules partitioned to the benzene phase. When the aqueous phase was used for the subsequent selection round, plaque formation was observed, at both the second and the third rounds of selection. This result indicates that dissociation of the perylene crystal particles into their constituent monomers might have facilitated the separation of the peptide-displaying phages from perylene. We analyzed survival of phages in the mixture of benzene and aqueous solution: the influence of benzene little decreased phage titer

(Fig. S1 in ESI[†]). This demonstrates little effect of the benzene used on the infectivity of the phages.

The peptides selected by biopanning with acidic desorption or with liquid-liquid extraction are listed in Table 1. Three different peptides were identified in the plaques generated *via* the acidic desorption method (PeryBP_{g1-3}), and *E. coli* infected by the phages without bound peptide also formed plaques. In contrast, all the plaques generated by infection of *E. coli* with phages selected by biopanning with liquid-liquid extraction contained a single peptide (PeryBP_{b1}). This result indicates that the liquid-liquid extraction method facilitated separation of

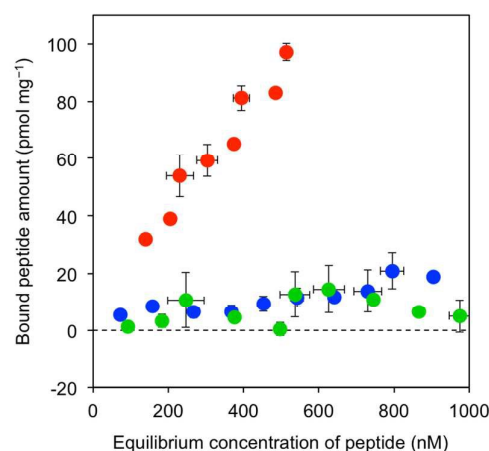


Fig. 3 Adsorption isotherms for binding of PeryBP_{g1} (blue circles), PeryBP_{g2} (green circles), and PeryBP_{b1} (red circles) to perylene crystals (5 mg mL⁻¹) in 10 mM sodium phosphate solution (pH 7.5). Each plot was measured three times and the presented results correspond to averages with error bars.

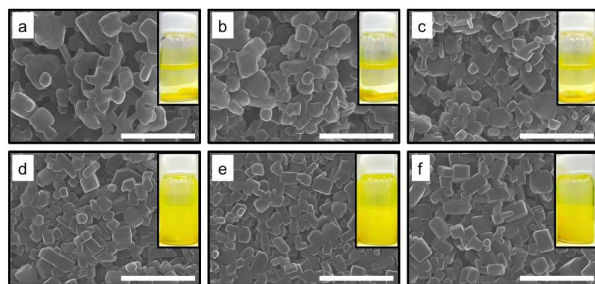


Fig. 4 Effect of PeryBP_{b1} for dispersity and morphology of the perylene crystals that prepared by reprecipitation method. SEM images of perylene crystals prepared by various concentration of PeryBP_{b1} peptide (0–100 μM). Each particle was formed at the PeryBP_{b1} concentration of 0 μM (a), 5 μM (b), 12.5 μM (c), 25 μM (d), 50 μM (e), and 100 μM (f). The images were measured at acceleration voltages of 20 kV. Scale bars = 1 μm. Inset: photographs of the perylene crystals suspension with each concentration of PeryBP_{b1}. The crystal structures were gradually transformed to have edges with rise of the PeryBP_{b1} concentrations.

the peptide-displaying phages from the perylene crystal particles.

Assay of the binding affinity of the selected peptides

To evaluate the binding affinity of the selected peptides, we measured adsorption isotherms for interaction of the peptides with perylene crystal particles (Fig. 3). Each of the three highly amplified peptides (PeryBP_{g1}, PeryBP_{g2}, and PeryBP_{b1}) was conjugated with a fluorescein molecule at the N-terminus and then mixed with perylene crystals. After centrifugation of the mixture, the residual fluorescence in the supernatant was measured. The adsorption isotherms were transformed to Langmuir plots to estimate the equilibrium dissociation constants (K_d) (Table 1, Fig. S2a in ESI[†]). The three peptides did bind to the perylene crystal particles, but the bound amounts of the two peptides obtained *via* the acidic desorption method were too low to estimate the equilibrium dissociation constants (K_d) from the Langmuir plots. In contrast, PeryBP_{b1}, which was obtained by the liquid–liquid extraction method, bound to the perylene particles with a K_d value of 1.1 μM. This result indicates that the liquid–liquid extraction method led to isolation of phages bearing a peptide that bound to perylene more tightly than the peptides obtained *via* the acidic desorption method.

Effect of crystal-binding peptide PeryBP_{b1} on the morphology of crystalline perylene nanoparticles

To analyze how the binding of PeryBP_{b1} influenced the formation of perylene crystal particles, we rapidly diluted a

dimethylsulfoxide solution of perylene either in water alone or in an aqueous solution containing PeryBP_{b1} at various concentrations. In the absence of PeryBP_{b1}, perylene crystal particles aggregated and precipitated spontaneously (Fig. 4a). In contrast, when the concentration of PeryBP_{b1} in the aqueous solution was ≥ 25 μM, the crystal particles that formed remained dispersed in the solution, indicating that the surface of the perylene–PeryBP_{b1} crystal particles was more hydrophilic than that of the unadorned perylene crystal particles (Fig. 4d–f). SEM images of the crystal particles formed in water and in the aqueous solutions containing PeryBP_{b1} at various concentrations indicated that in the absence of PeryBP_{b1}, the size and morphology of the perylene crystal particles were heterogeneous and that partial fusion of the crystals occurred. As the PeryBP_{b1} concentration was increased, the particle size decreased to ca. 250 nm, and the particles changed from heterogeneous spherical shapes to relatively homogenous planar structures. That is, the presence of PeryBP_{b1} decreased the size and changed the morphology of the perylene crystal particles. The acceleration voltages for measuring SEM images were changed in the range of 3–15 kV, and no structural changes of crystal particles were observed (Fig. S3 in ESI[†]). The structures of formed perylene particles were stable for the applied electron beam. In addition, we conducted TEM analysis of the perylene crystals. Although the use of high acceleration voltage changed the shapes of perylene crystal particles slightly, the TEM images supported the results of SEM analysis (Fig. S4 in ESI[†]).

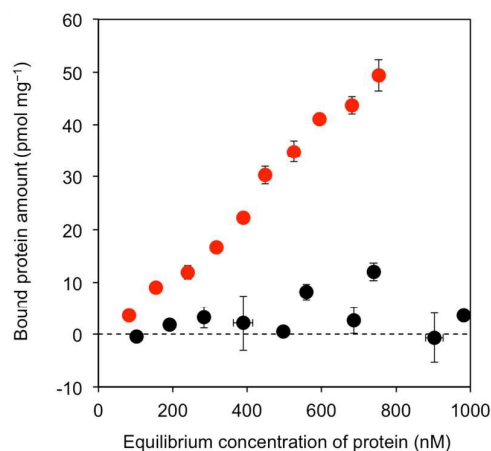


Fig. 5 Adsorption isotherms for binding of PeryBP_{b1}-fused DsRed-Monomer (red circles) and DsRed-Monomer (control, black circles) to perylene crystals (5 mg mL⁻¹) in 10 mM sodium phosphate solution (pH 7.5). Each plot was measured three times and the presented results correspond to averages with error bars.

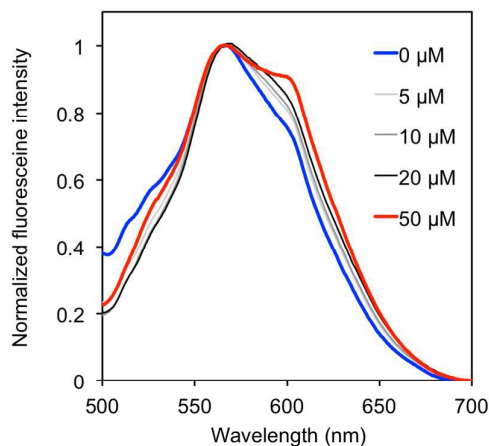


Fig. 6 Concentration dependence of emission spectra of DsRed-Monomer immobilized on perylene crystals at an excitation wavelength of 400 nm at PeryBP_{b1}-fused DsRed-Monomer concentrations of 0, 5, 10, 20, and 50 μM , respectively. We confirmed that emission of DsRed-monomer was not observed by excitation wavelength at 400 nm (Fig. S6 in ESI[†]). As concentration of DsRed-Monomer increased, the bands at 587 nm derived from the emission of DsRed-Monomer were gradually raised, which results suggested that the energy of perylene crystals transferred to DsRed-Monomer.

X-ray diffraction of the perylene crystals prepared with

PeryBP_{b1} was also measured; however, the diffraction was the same pattern of α -form as that of the perylene crystals prepared without PeryBP_{b1}. This indicates that the interaction of PeryBP_{b1} is not enough strong to change the crystal form. PeryBP_{b1} bound onto the surface of perylene crystal particles just as capping agents.

Protein immobilization on crystalline perylene nanoparticles

To immobilize a protein on the perylene crystal particles, we fused PeryBP_{b1} to the N-terminus of the red fluorescent protein DsRed-Monomer, which is derived from *Discosoma*. DsRed-Monomer has the potential of energy acceptor from perylene crystals because of the overlapping of emission spectra of perylene crystal with an excitation band of DsRed-Monomer (Fig. S5 in ESI[†]); whereas, fluorescein with absorbance at 495 nm hardly cause FRET with perylene crystals. To evaluate the potential of PeryBP_{b1} as an anchoring tag, we analyzed the binding affinity of PeryBP_{b1}-fused DsRed-Monomer for perylene crystal particles (Fig. 5). We found that at saturation, the amount of adsorbed DsRed-Monomer was about one-third that of fluorescein-conjugated PeryBP_{b1} ($W_s = 67 \text{ pmol mg}^{-1}$), perhaps owing to steric interactions between the adsorbed proteins. In contrast, the PeryBP_{b1}-fused DsRed-Monomer bound to the crystal particles with a K_d value comparable to that of fluorescein-conjugated PeryBP_{b1} (1.5 μM). These parameters were calculated by Langmuir plot (Fig. S2b in ESI[†]). That is, PeryBP_{b1} could bind to perylene crystal particles and act as a tag at the terminus of the protein.

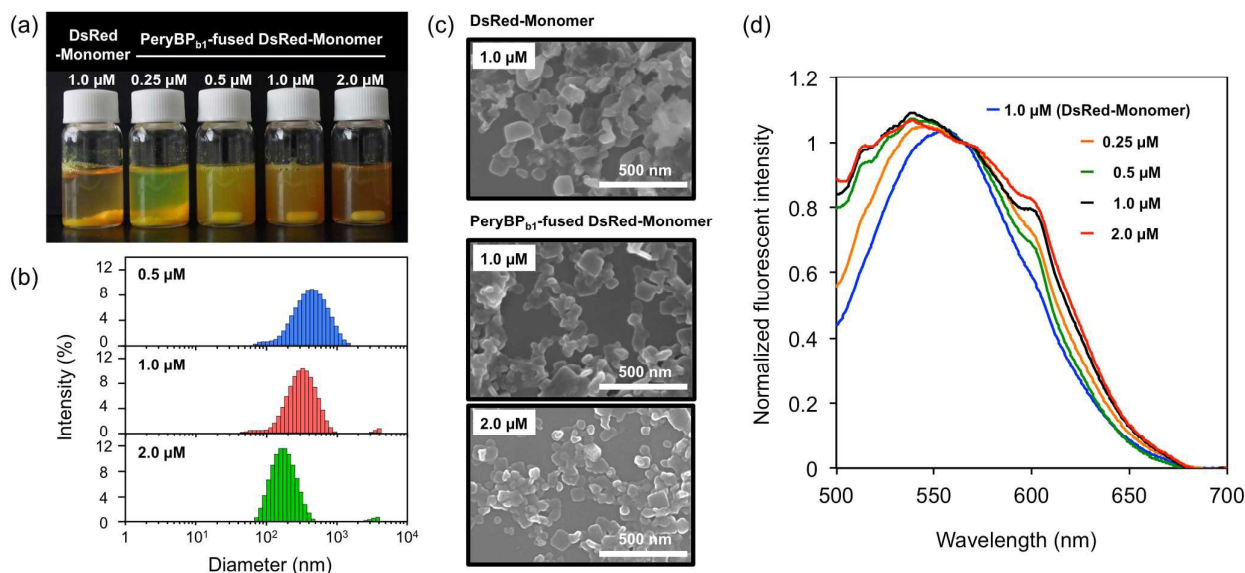


Fig. 7 Perylene crystal particles suspension prepared by reprecipitation method with PeryBP_{b1}-fused DsRed-Monomer concentration of 0.25 μM , 0.5 μM , 1.0 μM , and 2.0 μM or 1.0 μM DsRed-Monomer absence of PeryBP_{b1}. Image of the perylene crystal particles suspension (a), particle size distribution of the perylene crystals measured by DLS (b), SEM images of the perylene crystals (c), and emission spectra of DsRed-Monomer immobilized on perylene crystals with the excitation wavelength of 400 nm (d). In DLS analysis, average diameters and polydispersity index of each sample were 379 nm and 0.279 (blue), 291 nm and 0.250 (red), and 170 nm and 0.208 (green), respectively. In SEM analysis, the measurements were conducted with 5 kV of acceleration voltages.

Upon excitation at 556 nm, DsRed-Monomer exhibits an emission band at 587 nm (Fig. S5 in ESI[†]), which is not observed upon excitation at 400 nm (Fig. S6 in ESI[†]). Perylene crystal particles show broad emission bands around 565 nm upon excitation at 400 nm. In this study, we mixed PeryBP_{b1}-fused DsRed-Monomer with perylene crystal particles at various concentrations and then measured the emission spectra of DsRed-Monomer to detect FRET from the perylene crystal particles to DsRed-Monomer upon excitation at 400 nm (Fig. 6). When all the emission spectra were normalized by the emission intensity at 565 nm, the emission intensity around 587 nm gradually increased as the concentration of PeryBP_{b1}-fused DsRed-Monomer increased. That is, the binding of DsRed-Monomer to the perylene crystal particles *via* PeryBP_{b1} brought the DsRed-Monomer and perylene sufficiently close to each other to allow FRET.

One-pot formation of protein-immobilized crystalline perylene nanoparticles

We carried out the one-pot formation of protein-immobilized crystalline perylene nanoparticles. A dimethylsulfoxide solution of perylene was added to 10 mM sodium phosphate buffer (pH 7.5) alone or 10 mM sodium phosphate buffer containing PeryBP_{b1}-fused DsRed-Monomer at various concentrations. In the presence of peptide-unfused DsRed-Monomer, the formed crystal nanoparticles were aggregated (Fig. 7a, 1.0 μM DsRed-Monomer). The aggregations were also observed for the formation of perylene particles in the presence of bovine serum albumin (BSA) and lysozyme (Fig. S7 in ESI[†]). In contrast, when the PeryBP_{b1}-fused DsRed-Monomer concentration was ≥0.5 μM, the formed crystalline nanoparticles were dispersed, and at 2 μM the solution was transparent (Fig. 7a, 0.25–2.0 μM PeryBP_{b1}-fused DsRed-Monomer). That is, the hydrophilicity of the bound DsRed-Monomer increased the dispersibility of the formed crystalline nanoparticles.

We used DLS and SEM to evaluate the structure of the crystalline perylene nanoparticles (Fig. 7b and c). The distribution of hydrodynamic diameters determined by DLS showed a gradual decrease in size to less than 200 nm with increasing PeryBP_{b1}-fused DsRed-Monomer concentration. Considering that the hydrodynamic diameter of the crystalline nanoparticles formed in the presence of PeryBP_{b1} was more than 1 μm (data not shown), our results show that fusion of the protein to PeryBP_{b1} drastically decreased the diameter of the crystalline nanoparticles. In the SEM images, the crystalline nanoparticles formed in the presence of peptide-unfused DsRed-Monomer, BSA, and lysozyme, were smaller than the nanoparticles formed in the absence of the proteins (perhaps owing to a weak interaction between perylene and protein), and the nanoparticles adhered to one another (1.0 μM peptide-unfused DsRed-Monomer in Fig. 7c, and Fig. S7 in ESI[†]). In contrast, the presence of PeryBP_{b1}-fused DsRed-Monomer led to an additional decrease in the particle diameter and prevented adhesion of the nanoparticles (Fig. 7c, 1.0 and 2.0 μM). The fusion of the protein to PeryBP_{b1} decreased the size and increased the hydrophilicity of the crystalline nanoparticles.

We also measured FRET from perylene to DsRed-Monomer for the crystalline nanoparticles formed with PeryBP_{b1}-fused DsRed-Monomer (Fig. 7d). In the fluorescence spectra moralized at an emission wavelength of 565 nm, the emission intensity around 587 nm gradually increased as the concentration of PeryBP_{b1}-fused DsRed-Monomer was increased. PeryBP_{b1}-fused DsRed-Monomer was immobilized on the perylene crystal particles with its fluorescent activity retained. That is, the fusion of the crystal-binding peptide to the protein enabled one-pot formation of protein-immobilized organic crystal nanoparticles.

Discussion

Liquid–liquid extraction as a new elution method for phage display systems

Peptide libraries based on phage display and cell surface technologies have been used to select peptides with affinity for the surfaces of various materials. In this study, we selected perylene-crystal-binding peptides by means of a modified biopanning approach in which phages bound to perylene crystal particles were eluted by dissolution of the perylene crystals in benzene. Giordano *et al.* used a water-insoluble heavy organic solvent to separate phages from target-displaying cells;³⁵ specifically, a cell suspension incubated with phages in an aqueous upper phase was centrifuged through an immiscible organic lower phase, and the cell-bound phages were then collected from the cells. In this study, the addition of benzene to the aqueous phase containing crystal-bound phages resulted in dissolution of the perylene crystals and distribution of the perylene molecules to the benzene phase. Because the phages were predominantly distributed to the water phase, this method allowed the selection of crystal-binding peptides from the peptide-displaying phage library.

Characteristics of the selected crystal-binding peptides

We calculated the hydropathy indexes of the four selected peptides to obtain information about their interactions with perylene (Table 1). Contrary to our expectations, PeryBP_{g1–3} and PeryBP_{b1} were hydrophilic, which is surprising considering that perylene is hydrophobic. Serizawa *et al.* identified some peptides with affinity for poly(methyl methacrylate),⁷ and the hydropathy indexes indicated that most of the peptides were hydrophilic. Considering that poly(methyl methacrylate) has ester groups, it is not surprising that peptides containing hydrophilic amino acids that can interact with the ester groups would be selected from the peptide library. In contrast, perylene is composed solely of carbon and hydrogen atoms and cannot form hydrogen bonds with peptides. However, perylene has an aromatic structure and can therefore interact with conjugative structures, including those in the side chains of amino acids containing aromatic groups and double-bonded structures.³⁶ In fact, PeryBP_{b1}, which had the highest affinity for the perylene crystal particles, has 5 amino acid residues with conjugative structures in the side chains (glutamine, histidine, asparagine, tyrosine, and arginine). The dispersion

force electrons might have interacted with the surface of the perylene crystal particles.

Control of nanostructure morphology by the crystal-binding peptides

Some peptides with affinity for inorganic materials can catalyze the synthesis of those materials. For example, addition of gold- or silver-binding peptides to a solution containing the corresponding metal ion induces spontaneous formation of nanoparticles with a specific crystal face,^{8,37} and ZnO-binding peptides can mediate the formation of ZnO nanocrystallites that assemble into unique flower-like structures.⁵ Recently, peptides with affinity for a specific crystal face of inorganic materials have been identified, and these peptides have been used for controlling the shapes of nanoparticles of the materials. Chiu *et al.* selected platinum-binding peptides from phage libraries by using a silicon substrate with an exposed platinum crystal face as a target.¹⁷ Addition of the peptides to a reductive solution for platinum synthesis led to the formation of nanoparticles with only the corresponding crystal face. In the case of ceramics, suppression of (0001) growth in ZnO crystals by a dipeptide with affinity for ZnO has been reported.³⁸

To our knowledge, control of the morphology of organic crystals by means of material-binding peptides has not previously been reported. Here, we identified peptides that could bind to perylene crystal particles with planar shapes and consisting predominantly of the (001) crystal face (Fig. 1). The presence of the crystal-binding peptides during the formation of perylene crystals resulted in relatively homogenous planar structures, indicating the capping effect of the peptides on the (001) crystal face. Enhancement of the binding affinity of the crystal-binding peptide might allow even better morphological control by means of this capping effect.

In addition to controlled morphology, dispersion of particles in solution is also essential for their various uses.³⁰ Here, we found that the presence of a crystal-binding peptide suppressed precipitation of perylene crystals owing to an increase in hydrophilicity due to binding of the peptide. Furthermore, the use of peptide-fused proteins promoted the hydrophilicity, and a functional peptide-fused protein could be spontaneously immobilized on the perylene crystal particles. Material-binding peptides have been used for protein immobilization on patterned substrates and nanoparticles because the N- or C-terminus of peptides can be fused to proteins by means of genetic techniques.^{11–14,39–41} We showed that one of the selected peptides, PeryBP_{b1}, could be used for protein immobilization. The increase in dispersibility imparted by the peptide and its successful use for protein immobilization suggest that the peptide could be used to produce organic nanocrystals for bioimaging by enhancing the binding affinity of the peptide for nanocrystals.

Conclusions

We selected several peptides with affinity for perylene crystal particles from a phage library by means of a liquid–liquid

extraction method. One of the selected peptides could be used to disperse perylene crystal particles in an aqueous solution and to control crystal formation by a poor solvent method. DsRed-Monomer fused to the peptide could be spontaneously immobilized on perylene crystal particles at a distance close enough to permit FRET between the perylene crystals and DsRed-Monomer. The FRET result indicates the potential of combination between organic crystals and protein. Our results show that peptides can recognize the surface of molecular assemblies formed by small organic molecules and can be used to control the morphology and dispersion of organic crystal particles water, as well as for one-pot protein immobilization.

Acknowledgements

This work was partly supported by a Scientific Research Grant from the Ministry of Education, Science, Sports, and Culture of Japan (M.U., I.K.), and by funding from the Precursory Research for Embryonic Science and Technology program of the Japan Science and Technology (JST) Agency (M.U.). This work was also partially supported by the Asahi Glass Foundation. We thank Mr. Kayamori, Ms. Arakawa, Mr. Miyazaki and Prof. Nagao for their help of measuring SEM and XRD.

References

- 1 S. Brown, *Nat. Biotechnol.*, 1997, **15**, 269–272.
- 2 K. I. Sano and K. Shiba, *J. Am. Chem. Soc.*, 2003, **125**, 14234–14235.
- 3 S. R. Whaley, D. S. English, E. L. Hu, P. F. Barbara and a M. Belcher, *Nature*, 2000, **405**, 665–668.
- 4 S. Brown, *Proc. Natl. Acad. Sci. U. S. A.*, 1992, **89**, 8651–8655.
- 5 M. Umetsu, M. Mizuta, K. Tsumoto, S. Ohara, S. Takami, H. Watanabe, I. Kumagai and T. Adschiri, *Adv. Mater.*, 2005, **17**, 2571–2575.
- 6 E. E. Oren, C. Tamerler, D. Sahin, M. Hnilova, U. O. S. Seker, M. Sarikaya and R. Samudrala, *Bioinformatics*, 2007, **23**, 2816–2822.
- 7 T. Serizawa, T. Sawada, H. Matsuno, T. Matsubara and T. Sato, *J. Am. Chem. Soc.*, 2005, **127**, 13780–13781.
- 8 R. R. Naik, S. J. Stringer, G. Agarwal, S. E. Jones and M. O. Stone, *Nat. Mater.*, 2002, **1**, 169–172.
- 9 C. Mao, D. J. Solis, B. D. Reiss, S. T. Kottmann, R. Y. Sweeney, A. Hayhurst, G. Georgiou, B. Iverson and A. M. Belcher, *Science*, 2004, **303**, 213–217.
- 10 Y. Shimada, M. Suzuki, M. Sugiyama, I. Kumagai and M. Umetsu, *Nanotechnology*, 2011, **22**, 275302.
- 11 T. Kacar, M. T. Zin, C. So, B. Wilson, H. Ma, N. Gul-Karaguler, A. K. Y. Jen, M. Sarikaya and C. Tamerler, *Biotechnol. Bioeng.*, 2009, **103**, 696–705.
- 12 M. Hnilova, C. R. So, E. E. Oren, B. R. Wilson, T. Kacar, C. Tamerler and M. Sarikaya, *Soft Matter*, 2012, **8**, 4327–4334.
- 13 S. Brown, *Nano Lett.*, 2001, **1**, 391–394.
- 14 W. Zhou, D. T. Schwartz and F. Baneyx, *J. Am. Chem. Soc.*, 2010, **132**, 4731–4738.
- 15 R. M. Kramer, C. Li, D. C. Carter, M. O. Stone and R. R. Naik, *J. Am. Chem. Soc.*, 2004, **126**, 13282–13286.
- 16 C. L. Chen, P. Zhang and N. L. Rosi, *J. Am. Chem. Soc.*, 2008, **130**, 13555–13557.
- 17 C.-Y. Chiu, Y. Li, L. Ruan, X. Ye, C. B. Murray and Y. Huang, *Nat. Chem.*, 2011, **3**, 393–399.

- 18 M. Jazbinsek, L. Mutter and P. Gunter, *IEEE J. Sel. Top. Quantum Electron.*, 2008, **14**, 1298–1311.
- 19 X. Zhang, X. Zhang, W. Shi, X. Meng, C. Lee and S. Lee, *J. Phys. Chem. B*, 2005, **109**, 18777–18780.
- 20 Y. Lei, Q. Liao, H. Fu and J. Yao, *J. Phys. Chem. C*, 2009, **113**, 10038–10043.
- 21 X. Wang, H. Li, Y. Wu, Z. Xu and H. Fu, *J. Am. Chem. Soc.*, 2014, **136**, 16602–16608.
- 22 J. E. Park, M. Son, M. Hong, G. Lee and H. C. Choi, *Angew. Chem. Int. Ed. Engl.*, 2012, **51**, 6383–8.
- 23 Q. H. Cui, Y. S. Zhao and J. Yao, *Adv. Mater.*, 2014, 6852–6870.
- 24 R. T. Weitz, K. Amsharov, U. Zschieschang, E. B. Villas, D. K. Goswami, M. Burghard, H. Dosch, M. Jansen, K. Kern and H. Klauk, *J. Am. Chem. Soc.*, 2008, **130**, 4637–4645.
- 25 A. S. Molinari, H. Alves, Z. Chen, A. Facchetti and A. F. Morpurgo, *J. Am. Chem. Soc.*, 2009, **131**, 2462–2463.
- 26 M. Gsänger, J. H. Oh, M. Könemann, H. W. Höffken, A. M. Krause, Z. Bao and F. Würthner, *Angew. Chem. Int. Ed.*, 2010, **49**, 740–743.
- 27 A. L. Briseno, S. C. B. Mannsfeld, C. Reese, J. M. Hancock, Y. Xiong, S. A. Jenekhe, Z. Bao and Y. Xia, *Nano Lett.*, 2007, **7**, 2847–2853.
- 28 S. Karak, S. K. Ray and A. Dhar, *Appl. Phys. Lett.*, 2010, **97**, 043306.
- 29 H. Kasai, H. Kamatani, S. Okada, H. Oikawa, H. Matsuda and H. Nakanishi, *Jpn. J. Appl. Phys.*, 1996, **35**, L221–L223.
- 30 A. L. Briseno, S. C. B. Mannsfeld, X. Lu, Y. Xiong, S. a. Jenekhe, Z. Bao and Y. Xia, *Nano Lett.*, 2007, **7**, 668–675.
- 31 H. Kasai, S. Nalwa, Hari, H. Oikawa, S. Okada, H. Matsuda, N. Minami, A. Kakuta, K. Ono, A. Mukoh and H. Nakanishi, *Jpn. J. Appl. Phys.*, 1992, **31**, L1132–L1134.
- 32 H. Kasai, H. Oikawa, S. Okada and H. Nakanishi, *Bull. Chem. Soc. Jpn.*, 1998, **71**, 2597–2601.
- 33 G. S. Waldo, B. M. Standish, J. Berendzen and T. C. Terwilliger, *Nat. Biotechnol.*, 1999, **17**, 691–695.
- 34 N. Yokoo, T. Togashi, M. Umetsu, K. Tsumoto, T. Hattori, T. Nakanishi, S. Ohara, S. Takami, T. Naka, H. Abe, I. Kumagai and T. Adschiri, *J. Phys. Chem. B*, 2010, **114**, 480–486.
- 35 R. J. Giordano, M. Cardó-Vila, J. Lahdenranta, R. Pasqualini and W. Arap, *Nat. Med.*, 2001, **7**, 1249–1253.
- 36 C. Steffen, K. Thomas, U. Huniar, A. Hellweg, O. Rubner and A. Schroer, *J. Comput. Chem.*, 2010, **31**, 2967–2970.
- 37 S. Brown, M. Sarikaya and E. Johnson, *J. Mol. Biol.*, 2000, **299**, 725–735.
- 38 T. Togashi, N. Yokoo, M. Umetsu, S. Ohara, T. Naka, S. Takami, H. Abe, I. Kumagai and T. Adschiri, *J. Biosci. Bioeng.*, 2011, **111**, 140–145.
- 39 E. Yuca, A. Y. Karatas, U. O. S. Seker, M. Gungormus, G. Dinler-Doganay, M. Sarikaya and C. Tamerler, *Biotechnol. Bioeng.*, 2011, **108**, 1021–1030.
- 40 T. Niide, K. Shimojo, R. Wakabayashi, M. Goto and N. Kamiya, *Langmuir*, 2013, **29**, 15596–15605.
- 41 T. Niide, M. Goto and N. Kamiya, *RSC Adv.*, 2014, **4**, 5995–5998.